Explanation of Bird Migration Using Ultimate Acceleration

Huaiyang Cui
Department of Physics, Beihang University, Beijing, 102206, China
Email: hycui@buaa.edu.cn
(November 1, 2022, submitted to viXra)

Abstract: In analogy with the ultimate speed c, there is an ultimate acceleration β, nobody's acceleration can exceed this limit β, in the solar system, β=2.961520e+10(m/s^2). Because this ultimate acceleration is large, any effect related to β will become easy to test, including quantum gravity tests. In this paper, an approach is put forward to connect the ultimate acceleration with quantum theory, and is applied to sunspot problems. The sunspot cycle is calculated to be 10.93 years due to the ultimate acceleration. Due to quantum effect of the ultimate acceleration, the atmospheric constructive interference condition takes place at certain latitudes where are traditional habitats of migratory birds, so this relativistic approach provides a direction guidance for bird migration.

1. Introduction

In general, some quantum gravity proposals [1,2] are extremely hard to test in practice, as quantum gravitational effects are appreciable only at the Planck scale [3]. But ultimate acceleration provides another scheme to deal with quantum gravity effects.

In analogy with the ultimate speed c, there is an ultimate acceleration β, nobody's acceleration can exceed this limit β, in the solar system, β=2.961520e+10(m/s^2). Because this ultimate acceleration is large, any effect related to β will become easy to test, including quantum gravity tests. In this paper, an approach is put forward to connect the ultimate acceleration with quantum theory, is applied to sunspot and earth's atmospheric circulation problems.

Birds migrate regularly and on a large scale every year, attracting human attention long ago. It is found that the atmospheric constructive interference condition takes place at certain latitudes where are traditional habitats of migratory birds, so this relativistic approach provides a direction guidance for bird migration.

2. How to connect the ultimate acceleration with quantum theory

In relativity, the speed of light c is the ultimate speed, nobody's speed can exceed this limit c. The relativistic velocity u of a particle in the coordinate system (x_1,x_2,x_3,x_4=ict) satisfies

$$u_1^2+u_2^2+u_3^2+u_4^2=-c^2 \quad . \tag{1}$$

No matter what particles (electrons, molecules, neutrons, quarks), their 4-vector velocities all have the same magnitude: $|u|=ic$. All particles gain **equality** because of the same magnitude of the 4-velocity u. The acceleration a of a particle is given by

$$a_1^2+a_2^2+a_3^2=a^2; \quad (a_4=0; \quad \because x_4=ict) \tag{2}$$

Assume that particles have an ultimate acceleration β as the limit, no particle can exceed this acceleration limit β. Subtracting both sides of the above equation by β^2, we have

$$a_1^2 + a_2^2 + a_3^2 - \beta^2 = a^2 - \beta^2; \qquad a_4 = 0 \tag{3}$$

It can be rewritten as

$$[a_1^{\,2} + a_2^{\,2} + a_3^{\,2} + 0 + (i\beta)^2]\frac{1}{1 - a^2/\beta^2} = -\beta^2 \tag{4}$$

Now, the particle has an acceleration whose five components are specified by

$$\begin{aligned} &\alpha_1 = \frac{a_1}{\sqrt{1 - a^2/\beta^2}}; \quad \alpha_2 = \frac{a_2}{\sqrt{1 - a^2/\beta^2}}; \\ &\alpha_3 = \frac{a_3}{\sqrt{1 - a^2/\beta^2}}; \quad \alpha_4 = 0; \quad \alpha_5 = \frac{i\beta}{\sqrt{1 - a^2/\beta^2}}; \end{aligned} \tag{5}$$

where α_5 is the newly defined acceleration in five-dimensional space-time (x_1,x_2,x_3,x_4=ict,x_5). Thus, we have

$$\alpha_1^2 + \alpha_2^2 + \alpha_3^2 + \alpha_4^2 + \alpha_5^2 = -\beta^2; \quad \alpha_4 = 0 \tag{6}$$

It means that the magnitude of the newly defined acceleration α for every particle takes the same value: $|\alpha| = i\beta$ (constant imaginary number), all particle accelerations gain **equality** for the sake of the same magnitude.

How do resolve the velocity u and acceleration α into x, y, and z components? In a realistic world, a hand can rotate a ball moving around a circular path at constant speed v with constant centripetal acceleration a, as shown in Fig.1(a). Likewise, the u and α let the particle move spirally, as shown in Fig.1(b), projecting out the real x, y, and z components.

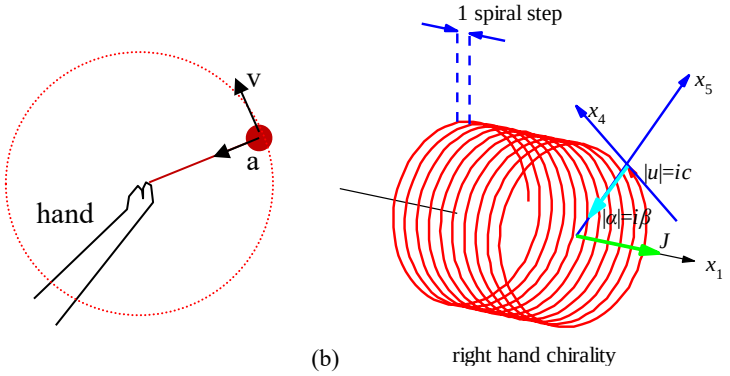

Fig.1 (a) A hand rotates a ball moving around a circular path at constant speed v with constant centripetal acceleration a. (b) The particle moves along the x_1 axis with the constant speed $|u| = ic$ in u direction and constant centripetal force in the x_5 axis at the radius iR (imaginary number).

```
<Clet2020 Script>//[26]
double D[100],S[2000];int i,j,R,X,N;
int main(){R=50;X=50;N=600;D[0]=-50;D[1]=0;D[2]=0;D[3]=X;D[4]=0;D[5]=0;D[6]=-50;D[7]=R;D[8]=0;
D[9]=600;D[10]=10;D[11]=R;D[12]=0;D[13]=3645;
Lattice(SPIRAL,D,S);SetViewAngle(0,80,-50);DrawFrame(FRAME_NULL,1,0xffffff);
Draw("LINE,0,2,XYZ,0","-150,0,0,-50,0,0");Draw("ARROW,0,2,XYZ,10","50,0,0,150,0,0");
SetPen(2,0xff0000);Plot("POLYLINE,0,600,XYZ",S[9]);i=9+3*N-6;Draw("ARROW,0,2,XYZ,10",S[i]);
TextHang(S[i],S[i+1],S[i+2]," #if|u|=ic#t");TextHang(150,0,0," #ifx#sd1#t");SetPen(2,0x005fff);
Draw("LINE,1,2,XYZ,8","-50,0,50,-50,0,100");Draw("LINE,1,2,XYZ,8","-40,0,50,-40,0,100");
Draw("ARROW,0,2,XYZ,10","-80,0,100,-50,0,100");Draw("ARROW,0,2,XYZ,10","-10,0,100,-40,0,100");
TextHang(-50,0,110,"1 spiral step");i=9+3*N;S[i]=50;S[i+1]=10;S[i+2]=10;
Draw("ARROW,0,2,XYZ,10","50,0,0,50,80,80");TextHang(50,80,80," #ifx#sd5#t");
Draw("ARROW,0,2,XYZ,10","50,72,0,50,0,72");TextHang(50,0,72," #ifx#sd4#t");
SetPen(3,0x00ffff);Draw("ARROW,0,2,XYZ,15",S[i-3]);TextHang(S[i],S[i+1],S[i+2]," #if|α|=iβ#t");
SetPen(3,0x00ff00);Draw("ARROW,0,2,XYZ,15","50,0,0,120,0,0");TextHang(110,5,5," #ifJ#t");
```

In analogy with the ball in a circular path, consider a particle in one-dimensional motion along the x_1 axis at the speed v, in Fig.1(b) it moves with the constant speed $|u|=ic$ almost along the x_4 axis and slightly along the x_1 axis, and the constant centripetal acceleration $|\alpha|=i\beta$ in the x_5 axis at the constant radius iR (imaginary number); the coordinate system (x_1,$x_4=ict$,$x_5=iR$) establishes a cylinder coordinate system in which this particle moves spirally at the speed v along the x_1 axis. According to the usual centripetal acceleration formula $a=v^2/r$, the acceleration in the x_4-x_5 plane is given by

$$a=\frac{v^2}{r} \quad \Rightarrow \quad i\beta=\frac{|u|^2}{iR}=-\frac{c^2}{iR}=i\frac{c^2}{R} \ . \tag{7}$$

Therefore, the track of the particle in the cylinder coordinate system (x_1,$x_4=ict$,$x_5=iR$) forms a shape, called **acceleration-roll**. The faster the particle moves along the x_1 axis, the longer the spiral step is.

Like a steel spring that contains an elastic wave, the track in the acceleration-roll in Fig.1(b) can be described by a wave function whose phase changes 2π for one spiral step. Apparently, this wave is just the de Broglie's matter wave for electrons, protons or quarks, etc.

Theorem: the acceleration-roll bears matter wave.

$$\psi=\exp(i\frac{\beta}{c^3}\int_0^x(u_1dx_1+u_2dx_2+u_3dx_3+u_4dx_4)) \ . \tag{8}$$

Proof: See ref. [28,30].

Depending on the particle under investigation, this wave function may have different explanations. If the β is replaced by the Planck constant, the wave function of electrons is given by

$$\begin{aligned} &assume: \quad \beta=\frac{mc^3}{\hbar} \\ &\psi=\exp(\frac{i}{\hbar}\int_0^x(mu_1dx_1+mu_2dx_2+mu_3dx_3+mu_4dx_4)) \end{aligned} \ . \tag{9}$$

where $mu_4dx_4=-Edt$, it strongly suggests that the wave function is just the de Broglie's matter wave [4,5,6].

Considering another explanation to ψ for planets in the solar system, no Planck constant can be involved. But, in a many-body system with the total mass M, the data analysis [28] tells us that the ultimate acceleration can be rewritten in terms of **Planck-constant-like constant** h as

$$\begin{aligned} &assume: \quad \beta=\frac{c^3}{hM} \\ &\psi=\exp(\frac{i}{hM}\int_0^x(u_1dx_1+u_2dx_2+u_3dx_3+u_4dx_4)) \end{aligned} \ . \tag{10}$$

The constant h will be determined by experimental observations. This paper will show that this wave function is applicable to several many-body systems in the solar system, the wave

function is called the **acceleration-roll wave**.

Tip: actually, ones cannot get to see the acceleration-roll of a particle in the relativistic space-time ($x_1,x_2,x_3,x_4=ict$) ; only get to see it in the cylinder coordinate system ($x_1,x_4=ict,x_5=iR$).

3. How to determine the ultimate acceleration

In Bohr's orbit model for planets or satellites, as shown in Fig.2, the circular quantization condition is given in terms of relativistic matter wave in gravity by

$$\left.\begin{aligned}\frac{\beta}{c^3}\oint_L v_l dl = 2\pi n \\ v_l = \sqrt{\frac{GM}{r}}\end{aligned}\right\} \Rightarrow \sqrt{r} = \frac{c^3}{\beta\sqrt{GM}}n; \quad n = 0,1,2,\ldots \ . \tag{11}$$

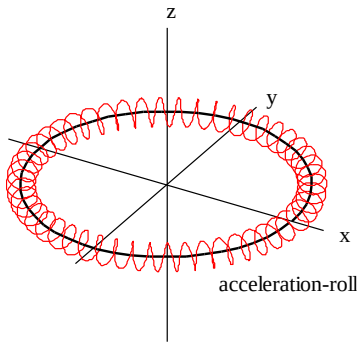

Fig.2 A planet 2D orbit around the sun, an acceleration-roll winding around the planet.

```
<Clet2020 Script>//[26]
int i,j,k; double r,rot,x,y,z,D[20],F[20],S[200]; int main(){SetViewAngle("temp0,theta60,phi-30");
DrawFrame(FRAME_LINE,1,0xafffaf);r=80;Spiral(); TextHang(r,-r,0,"acceleration-roll");
r=110;TextHang(r,0,0,"x");TextHang(0,r,0,"y");TextHang(0,0,r,"z");}
Spiral(){r=80;j=10;rot=j/r;k=2*PI/rot+1;
for(i=0;i<k;i+=1) {D[0]=x;D[1]=y;D[2]=z;D[6]=x;D[7]=y;D[8]=r;
x=r*cos(rot*i);y=r*sin(rot*i);z=0;if(i==0) continue;
SetPen(2,0x00);F[0]=D[0];F[1]=D[1];F[2]=x;F[3]=y;Draw("LINE,0,2,XY,",F);SetPen(1,0xff0000);
D[3]=x;D[4]=y;D[5]=z; D[9]=40;D[10]=10;D[11]=8;D[12]=0;D[13]=360;
Lattice(SPIRAL,D,S);Plot("POLYLINE,0,40,XYZ",S[9]);}
}#v07=?>A#t
```

The solar system, Jupiter's satellites, Saturn's satellites, Uranus' satellites, and Neptune's satellites as five different many-body systems are investigated with the Bohr's orbit model. After fitting observational data as shown in Fig.3, their ultimate accelerations are obtained in Table 1. The predicted quantization blue-lines in Fig.3(a), Fig.3(b), Fig.3(c), Fig.3(d) and Fig.3(e) agree well with experimental observations for those *inner constituent planets or satellites*.

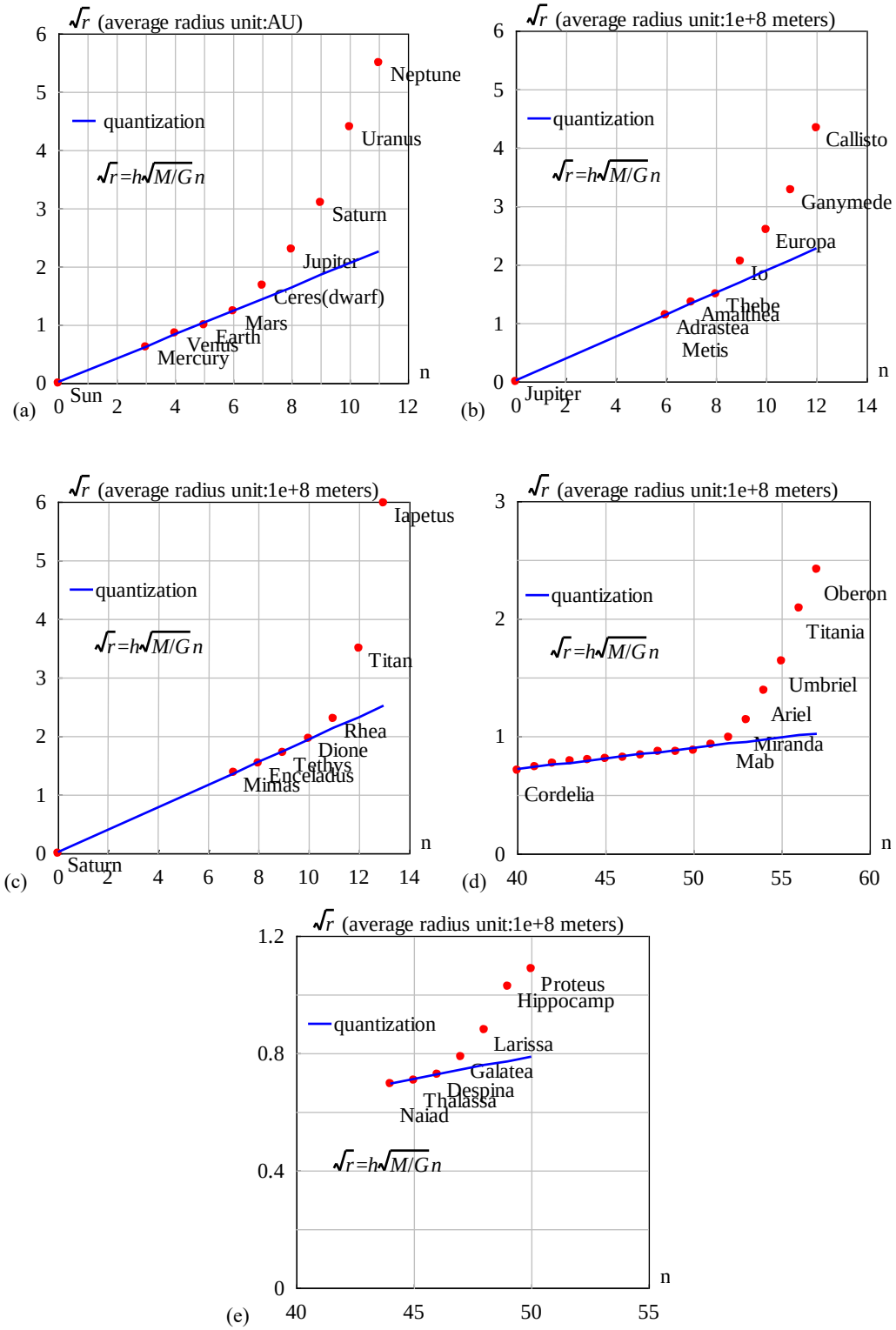

Fig.3 The orbital radii are quantized for inner constituents. (a) the solar system with h=4.574635e-16 ($m^2s^{-1}kg^{-1}$). The relative error is less than 3.9%. (b) the Jupiter system with h=3.531903e-16 ($m^2s^{-1}kg^{-1}$). Metis and Adrastea are assigned the same quantum number for their almost same radius. The relative error is less than 1.9%. (c) the Saturn system with h=6.610920e-16 ($m^2s^{-1}kg^{-1}$). The relative error is less than 1.1%. (d) the Uranus system with h=1.567124e-16 ($m^2s^{-1}kg^{-1}$). n=0 is assigned to Uranus. The relative error is less than 2.5%. (e) the Neptune system with h=1.277170e-16 ($m^2s^{-1}kg^{-1}$). n=0 is assigned to Neptune. The relative error is less than 0.17%.

Table 1 Planck-constant-like constant h, N is constituent particle number with smaller orbital inclination.

system	N	M/M_{earth}	β (m/s2)	h (m2s-1kg-1)	Prediction
Solar planets	9	333000	2.961520e+10	4.574635e-16	Fig.3(a)
Jupiter' satellites	7	318	4.016793e+13	3.531903e-16	Fig.3(b)
Saturn's satellites	7	95	7.183397e+13	6.610920e-16	Fig.3(c)
Uranus' satellites	18	14.5	1.985382e+15	1.567124e-16	Fig.3(d)
Neptune 's satellites	7	17	2.077868e+15	1.277170e-16	Fig.3(e)

Besides every β, our interest shifts to the constant h in Table 1, which is defined as

$$h=\frac{c^3}{M\beta} \quad \Rightarrow \quad \sqrt{r}=h\sqrt{\frac{M}{G}}n \ . \tag{12}$$

In a many-body system with a total mass of M, a constituent particle has the mass of m and moves at the speed of v, it is easy to find that the wavelength of de Broglie's matter wave should be modified for planets and satellites as

$$\lambda_{de\_Broglie}=\frac{2\pi\hbar}{mv} \quad \Rightarrow \text{modify} \Rightarrow \quad \lambda=\frac{2\pi hM}{v} \ . \tag{13}$$

where h is a **Planck-constant-like constant**. Usually, the total mass M is approximately equal to the central-star's mass. It is found that this modified matter wave works for quantizing orbits correctly in Fig.3 [28,29]. The key point is that the various systems have almost the same Planck-constant-like constant h in Table 1 with a mean value of 3.51e-16 $m^2s^{-1}kg^{-1}$, at least having the same magnitude! The acceleration-roll wave is a generalized matter wave on a planetary scale.

In Fig.3(a), the blue straight line expresses the linear regression relation among the Sun, Mercury, Venus, Earth and Mars, their quantization parameters are hM=9.098031e+14(m^2/s). The ultimate acceleration is fitted out to be β=2.961520e+10 (m/s^2). Where, n=3,4,5,.. were assigned to solar planets, the sun was assigned a quantum number n=0 because the sun is in the **central state**.

4. Optical model of the central state

The acceleration-roll wave as the relativistic matter wave generalized in gravity is given by

$$\psi=\exp(\frac{i}{hM}\int_0^x v_l dl); \quad \lambda=\frac{2\pi hM}{v_l}=\frac{2\pi c^3}{v_l\beta} \ . \tag{14}$$

In a central state n=0, if the coherent length of the acceleration-roll wave is long enough, its head may overlap with its tail when the particle moves in a closed orbit in space-time, as shown in Fig.4, the interference of the acceleration-roll wave between its head and tail will occur in the overlapping zone. The overlapped wave is given by

$$\psi(r)=1+e^{i\delta}+e^{i2\delta}+...+e^{i(N-1)\delta}=\frac{1-\exp(iN\delta)}{1-\exp(i\delta)}$$
$$\delta(r)=\frac{1}{hM}\oint_L(v_l)dl=\frac{2\pi\omega r^2}{hM}=\frac{2\pi\beta\omega r^2}{c^3} \quad . \tag{15}$$

where N is the overlapping number which is determined by the coherent length of the acceleration-roll wave, δ is the phase difference after one orbital motion, ω is the angular speed of the solar rotation. The above equation is a multi-slit interference formula in optics, for a larger N it is called the Fabry-Perot interference formula.

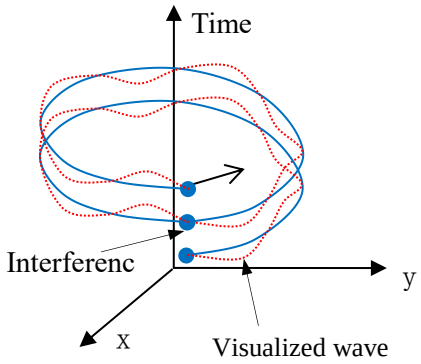

Fig.4 The head of the acceleration-roll wave may overlap with its tail.

The acceleration-roll wave function ψ needs a further explanation. In quantum mechanics, $|\psi|^2$ equals to the probability of finding an electron due to Max Burn's explanation; in astrophysics, $|\psi|^2$ equals to the probability of finding a nucleon (proton or neutron) *averagely on an astronomic scale*, because all mass is mainly made of nucleons, we have

$$|\psi|^2 \propto nucleon\_density \quad . \tag{16}$$

Comparing the solar core density with the atmospheric density, it was calculated that the solar overlapping number is N=341 [28,30]. The earth's overlapping number is N=65 [28,30].

Sun's angular speed at the equator is known as $\omega=2\pi/(25.05*24*3600)$, unit: s^{-1}. Its mass 1.9891e+30 (kg), radius 6.95e+8 (m), mean density 1408 (kg/m^3), the solar core has a maximum density of 1.5e+5kg/m^3 [31], the ultimate acceleration β=2.961520e+10 (m/s^2), the constant hM= 9.100745e+14 (m^2/s). According to the N=341, the matter distribution of the $|\psi|^2$ is calculated in Fig.5, it agrees well with the general description of the sun's interior. The radius of the sun is calculated to be r=7e+8 (m) with a relative error of 0.72% in Fig.5, which indicates that the sun radius strongly depends on the sun's self-rotation.

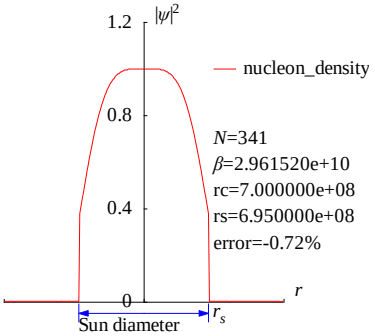

Fig.5 The matter distribution $|\psi|2$ around the Sun has been calculated in the radius direction.

```
<Clet2020 Script>//[26]
int i,j,k,m,n,N,nP[10];
double beta,H,B,M,r,r_unit,x,y,z,delta,D[1000],S[1000], a,b,rs,rc,rot,atm_height; char str[100];
main(){k=150;rs=6.95e8;rc=0;x=25.05;rot=2*PI/(x*24*3600);n=0; N=341;
beta=2.961520e10;H=SPEEDC*SPEEDC*SPEEDC/beta;M=1.9891E30; atm_height=2e6; r_unit=1E7;
b=PI/(2*PI*rot*rs*rs/H);
for(i=-k;i<k;i+=1) {r=abs(i)*r_unit;
if(r<rs+atm_height) delta=2*PI*rot*r*r/H; else delta=2*PI*sqrt(GRAVITYC*M*r)/H;//around the star
y=SumJob("SLIT_ADD,@N,@delta",D); y=y/(N*N);
S[n]=i;S[n+1]=y; if(i>0 && rc==0 && y<0.001) rc=r;D[n]=i;D[n+1]=z;n+=2;}
SetAxis(X_AXIS,-k,0,k,"#ifr; ; ; ;");SetAxis(Y_AXIS,0,0,1.2,"#if|ψ|#su2#t;0;0.4;0.8;1.2;");
DrawFrame(FRAME_SCALE,1,0xafffaf); z=100*(rs-rc)/rs;
SetPen(1,0xff0000);Polyline(k+k,S,k/2,1," nucleon_density"); SetPen(1,0x0000ff); //Polyline(k+k,D);
//Draw("LINE,0,2,XY,0","20,0.5,60,0.6");TextHang(60,0.6,0,"core");
r=rs/r_unit;y=-0.05;D[0]=-r;D[1]=y;D[2]=r;D[3]=y; Draw("ARROW,3,2,XY,10,100,10,10,",D);
Format(str,"#ifN#t=%d#n#ifβ#t=%e#nrc=%e#nrs=%e#nerror=%.2f%",N,beta,rc,rs,z);
TextHang(k/2,0.7,0,str);TextHang(r+5,y/2,0,"#ifr#sds#t");TextHang(-r,y+y,0,"Sun diameter");
}#v07=?>A#t
```

5. Earth's central state and space debris distribution

Appling the acceleration-roll wave to the Moon, as illustrated in Fig.6(a), the Moon has been assigned a quantum number of n=2 in the author's early study [28]. According to the quantum condition, the ultimate acceleration is fitted out to be β=1.377075e+14 (m/s^2) in the earth system. Another consideration is to take the quasi-satellite's perigee into account, for the moon and 2004_GU9 etc., as shown in Fig.6(b), but this consideration requires further understanding of its five quasi-satellites [28].

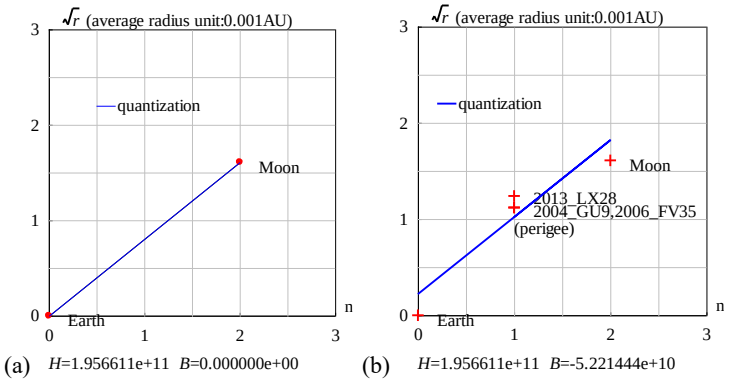

Fig.6 Orbital quantization for moon and quasi-satellites to the Earth, $H=hM$.

```
<Clet2020 Script>//[26]
char str[200];int i,j,k,N,nP[10]; double x,y,z,M,r_unit,a,b,B,H,r_ave[20],dP[10],D[1000];
double orbit[10]={0,2.57,0,}; double e[10]={0, 0.0549,0,0,0,0,0,0,0,0,};
int qn[10]={0,2,3,4,5,6,7,8,9.,10,}; char Stars[100]={"Earth;Moon;"};
int main(){ N=2; M=5.97237E24; r_unit=1.495978707e8;
for(i=0;i<N;i+=1) {x=orbit[i];y=e[i]; z=x*(1+sqrt(1-y*y))/2;r_ave[i]=z;//average_radius
D[i+i]=qn[i];D[i+i+1]=sqrt(z); }
DataJob("REGRESSION,2",D,dP);b=dP[0];a=dP[1];
SetAxis(X_AXIS,0,0,3,"n;0;1;2;3;");
SetAxis(Y_AXIS,0,0,3," #if#rsr#t (average radius unit:0.001AU);0;1;2;3;");
DrawFrame(0x0166,1,0xafffaf); Polyline(N,D);
SetPen(2,0xff0000); Plot("OVALFILL,0,2,XY,3,3,",D);
for(i=0;i<N;i+=1) {nP[0]=TAKE;nP[1]=i;TextJob(nP,Stars,str);x=qn[i]+0.2;y=sqrt(orbit[i])-0.05;TextHang(x,y,0,str);}
x=GRAVITYC*M*r_unit;z=sqrt(x);H=z*a;B=-z*b;
TextAt(100,450,"#ifH#t=%e  #ifB#t=%e",H,B);
for(i=0;i<N;i+=1) {y=b+a*qn[i];D[i+i]=qn[i];D[i+i+1]=y;}
SetPen(1,0x0000ff);Polyline(N,D,0.5,2.2,"quantization");//check
}}#v07=?>A#t
```

The earth's angular speed is known as ω=2π/(24*3600), unit s^{-1}. Its mass 5.97237e+24(kg), radius 6.371e+6(m), core density 5530(kg/m^3), the ultimate acceleration β=1.377075e+14(m/s^2), the constant hM=1.956611e+11(m^2/s).

Comparing the core density with the atmospheric density, it was calculated that the earth's

overlapping number is N=65 [28,30]. The matter distribution $|\psi|^2$ in radius direction is calculated as shown in Fig.7(a), where the self-rotation near its equator has the period of 24 hours:

$$\delta(r)=\frac{1}{hM}\oint_L(v_l)dl=\frac{2\pi r}{hM}\omega r=\frac{2\pi\beta\omega r^2}{c^3}\quad . \tag{17}$$

The matter distribution has a central maximum at the earth's heart, which gradually decreases to zero near the earth surface, then rises the secondary peaks and attenuates down off. The radius of the earth is calculated to be r=6.4328e+6 (m) with a relative error of 0.86% using the interference of its acceleration-roll wave. Space debris over the atmosphere has a complicated evolution [7,8], and has itself speed

$$v_l=\sqrt{\frac{GM}{r}};\quad \delta(r)=\frac{1}{hM}\oint_L(v_l)dl=\frac{\beta}{c^3}\oint_L(v_l)dl=\frac{2\pi\beta}{c^3}\sqrt{GMr}\quad . \tag{18}$$

The secondary peaks over the atmosphere up to 2000km altitude are calculated in Fig.7(b) which agree well with the space debris observations [16]; the peak near 890 km altitude is due principally to the January 2007 intentional destruction of the FengYun-1C weather spacecraft, while the peak centered at approximately 770 km altitude was created by the February 2009 accidental collision of Iridium 33 (active) and Cosmos 2251 (derelict) communication spacecraft [16,18]. The observations based on the incoherent scattering radar EISCAT ESR located at 78°N in Jul. 2006 and in Oct. 2015 [21,22,23] are respectively shown in Fig.7(c) and (d). This prediction of secondary peaks also agrees well with other space debris observations [24,25].

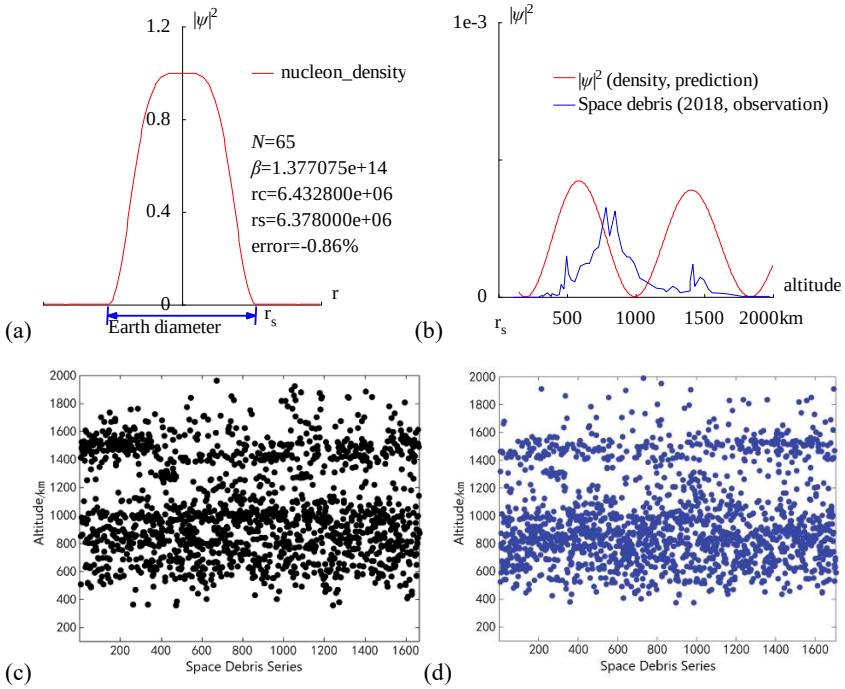

Fig.7 (a) The radius of the Earth is calculated out r=6.4328e+6 (m) with a relative error of 0.86% by the interference of its acceleration-roll wave; (b) The prediction of the space debris distribution up to 2000km altitude; (c) The pace debris distribution in Jul. 2006, Joint observation based on the incoherent scattering radar EISCAT ESR located at 78°N [21]; (d) The space debris distribution in Oct. 2015, Joint observation based on the incoherent scattering radar EISCAT ESR located at 78°N [21].

<Clet2020 Script>//[26]

```
int i,j,k,m,n,N,nP[10]; double H,B,M,v_r,r,AU,r_unit,x,y,z,delta,D[10],S[1000];
double rs,rc,rot,a,b,atm_height,beta; char str[100];
main(){k=80;rs=6.378e6;rc=0;atm_height=1.5e5;n=0; N=65;
beta=1.377075e+14;H=SPEEDC*SPEEDC*SPEEDC/beta;
M=5.97237e24;AU=1.496E11;r_unit=1e-6*AU; rot=2*PI/(24*60*60);//angular speed of the Earth
for(i=-k;i<k;i+=1) {r=abs(i)*r_unit;
if(r<rs+atm_height) v_r=rot*r*r; else v_r=sqrt(GRAVITYC*M*r);//around the Earth
delta=2*PI* v_r/H; y=SumJob("SLIT_ADD,@N,@delta",D); y=y/(N*N);
if(y>1) y=1; S[n]=i;S[n+1]=y; if(i>0 && rc==0 && y<0.001) rc=r;   n+=2;}
SetAxis(X_AXIS,-k,0,k,"r; ; ; ;");SetAxis(Y_AXIS,0,0,1.2,"#if|ψ|#su2#t;0;0.4;0.8;1.2;");
DrawFrame(FRAME_SCALE,1,0xafffaf); x=50;z=100*(rs-rc)/rs;
SetPen(1,0xff0000);Polyline(k+k,S,k/2,1," nucleon_density");
r=rs/r_unit;y=-0.05;D[0]=-r;D[1]=y;D[2]=r;D[3]=y;
SetPen(2,0x0000ff); Draw("ARROW,3,2,XY,10,100,10,10,",D);
Format(str,"#ifN#t=%d#n#ifβ#t=%e#nrc=%e#nrs=%e#nerror=%.2f%",N,beta,rc,rs,z);
TextHang(k/2,0.7,0,str);TextHang(r+5,y/2,0,"r#sds#t");TextHang(-r,y+y,0,"Earth diameter");
}#v07=?>A#t


<Clet2020 Script>//[26]
int i,j,k,m,n,N,nP[10]; double H,B,M,v_r,r,AU,r_unit,x,y,z,delta,D[10],S[10000];
double rs,rc,rot,a,b,atm_height,p,T,R1,R2,R3; char str[100]; int
Debris[96]={110,0,237,0,287,0,317,2,320,1,357,5,380,1,387,4,420,2,440,3,454,14,474,9,497,45,507,26,527,19,557,17,597,34,63
4,37,664,37,697,51,727,55,781,98,808,67,851,94,871,71,901,50,938,44,958,44,991,37,1028,21,1078,17,1148,10,1202,9,1225,6,
1268,12,1302,9,1325,5,1395,7,1395,18,1415,36,1429,12,1469,22,1499,19,1529,9,1559,5,1656,4,1779,1,1976,1,};
main(){k=80;rs=6.378e6;rc=0;atm_height=1.5e5;n=0; N=65;
H=1.956611e11;M=5.97237e24;AU=1.496E11;r_unit=1e4;
rot=2*PI/(24*60*60);//angular speed of the Earth
b=PI/(2*PI*rot*rs*rs/H); R1=rs/r_unit;R2=(rs+atm_height)/r_unit;R3=(rs+2e6)/r_unit;
for(i=R2;i<R3;i+=1) {r=abs(i)*r_unit; delta=2*PI*sqrt(GRAVITYC*M*r)/H;
y=SumJob("SLIT_ADD,@N,@delta",D); y=1e3*y/(N*N);// visualization scale:1000
if(y>1) y=1; S[n]=i;S[n+1]=y;n+=2;}
SetAxis(X_AXIS,R1,R1,R3,"altitude; r#sds#t;500;1000;1500;2000km ;");
SetAxis(Y_AXIS,0,0,1,"#if|ψ|#su2#t;0; ;1e-3;");DrawFrame(FRAME_SCALE,1,0xafffaf); x=R1+(R3-R1)/5;
SetPen(1,0xff0000);Polyline(n/2,S,x,0.8,"#if|ψ|#su2#t (density, prediction)");
for(i=0;i<48;i+=1) {S[i+i]=R1+(R3-R1)*Debris[i+i]/2000; S[i+i+1]=Debris[i+i+1]/300;}
SetPen(1,0x0000ff);Polyline(48,S,x,0.7,"Space debris (2018, observation) "); }#v07=?>A#t
```

6. Sunspot cycle

The **coherence length** of waves is usually mentioned but the **coherence width** of waves is rarely discussed in quantum mechanics, simply because the latter is not a matter for electrons, nucleon, or photons, but it is a matter in astrophysics. The analysis of observation data tells us that on the planetary scale, the coherence width of acceleration roll waves can be extended to 1000 kilometers or more, as illustrated in Fig.8(a), the overlap may even occur in the width direction, thereby bringing new aspects to wave interference.

In the solar convective zone, adjacent convective arrays form a top-layer flow, a middle-layer gas, and a ground-layer flow, similar to the concept of **molecular current** in electromagnetism. Considering one convective ring at the equator as shown in Fig.8(b), there is an apparent velocity difference between the top-layer flow and the middle-layer gas, where their acceleration-roll waves are denoted respectively by

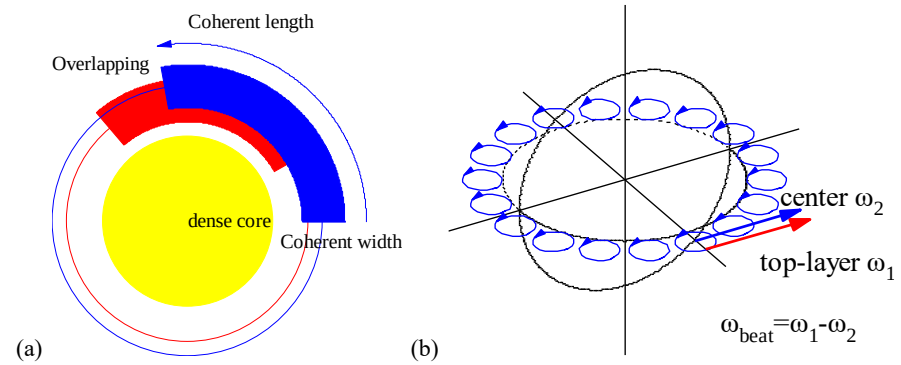

Fig.8 (a) Illustration of overlapping in the coherent width direction. (b) In convective rings at the equator, the speed difference causes a beat frequency.

```
<Clet2020 Script>// [26]
int i, j, k, R,D[500];
main(){DrawFrame(FRAME_NULL,1,0xafffaf);
R=60; SetPen(1,0xffff00);
D[0]=-R; D[1]=-R; D[2]=R; D[3]=R; Draw("ELLIPSE,1,2,XY,0",D);
R=85;   k=15; SetPen(1,0xff0000);
D[0]=-R; D[1]=-R; D[2]=R; D[3]=R; Draw("ELLIPSE,0,2,XY,0",D);
D[0]=0; D[1]=0; D[2]=R-k; D[3]=0; D[4]=R+k;D[5]=0;
Draw("SECTOR,1,3,XY,15,30,130,0",D);
R=95; k=15; SetPen(1,0x00ff);
D[0]=-R; D[1]=-R; D[2]=R; D[3]=R; Draw("ELLIPSE,0,2,XY,0",D);
D[0]=0; D[1]=0; D[2]=R-k; D[3]=0; D[4]=R+k;D[5]=0;
Draw("SECTOR,1,3,XY,15,0,100,0",D);D[4]=R+k+k;
Draw("SECTOR,3,3,XY,15,0,100,0",D);
TextHang(0,0,0,"dense core");TextHang(R-k-k,-k,0,"Coherent width");
TextHang(0,R+k+k+k,0,"Coherent length");TextHang(-R,R+k,0,"Overlapping");
}#v07=?>A#t
```

```
<Clet2020 Script>//Clet is a C compiler[26]
double beta,H,M,N,dP[20],D[2000],r,rs,rot,x,y,v1,v2,K1,K2,T1,T2,T,Lamda,L; int i,j,k;
int main(){beta=2.961520e10; H=SPEEDC*SPEEDC*SPEEDC/beta;
M=1.9891E30; rs=6.95e8;rot=2*PI/(25.05*24*3600);v1=rot*rs;K1=v1*v1/2;//T1=2*PI*H/K1;
v2=6100;//0.7346*sqrt(BOLTZMANN*5700/MP)+0.2485*sqrt(BOLTZMANN*5700/(MP+MP));
K2=v2*v2/2;T2=2*PI*H/(K2-K1);T=T2/24*3600*365.2422;
Lamda=2*PI*H/(v2-v1);L=2*PI*rs/Lamda;
SetViewAngle("temp0,theta60,phi-60");
DrawFrame(FRAME_LINE,1,0xaffffaf);Overlook("2,1,60", D);
TextAt(10,10,"v1=%d, v2=%d, T=%.2f y, #n λ=%e, L=%f",v1,v2,T, Lamda,L);
SetPen(1,0x4f4fff); for(i=0;i<18;i+=1) {v1=i*2*PI/18; x=70*cos(v1);y=70*sin(v1);Ring();}
SetPen(2,0xff0000);Draw("ARROW,0,2,XYZ,15","80,0,0,80,60,0");
TextHang(100,20,0,"top-layer ω#sd1#t"); SetPen(2,0x0000ff);
Draw("ARROW,0,2,XYZ,15","70,0,0,70,60,0");
TextHang(50,60,0,"center ω#sd2#t");TextHang(140,-30,0," ω#sdbeat#t=ω#sd1#t-ω#sd2#t");
}
Ring(){ k=0;N=20; r=10;
for(j=0;j<N+2;j+=1) {k=j+j+j; v2=j*2*PI/N;
D[k]=x+r*cos(v2);D[k+1]=y+r*sin(v2); D[k+2]=0;}
Plot("POLYLINE,4,22,XYZ,8",D);}
#v07=?>A
```

$$\psi = \psi_{top} + C\psi_{middle}$$

$$\psi_{top} = \exp[\frac{i\beta}{c^3}\int_L (v_1 dl + \frac{-c^2}{\sqrt{1-v_1^{\,2}/c^2}}dt)]$$

$$\psi_{middle} = \exp[\frac{i\beta}{c^3}\int_L (v_2 dl + \frac{-c^2}{\sqrt{1-v_2^{\,2}/c^2}}dt)] \qquad . \qquad (19)$$

Their interference in the coherent width direction leads to a beat phenomenon

$$|\psi|^2 = |\psi_{top} + C\psi_{middle}|^2 = 1 + C^2 + 2C\cos[\frac{2\pi}{\lambda_{beat}}\int_L dl - \frac{2\pi}{T_{beat}}t]$$

$$\frac{2\pi}{T_{beat}} = \frac{\beta}{c^3}(\frac{c^2}{\sqrt{1-v_1^{\,2}/c^2}} - \frac{c^2}{\sqrt{1-v_2^{\,2}/c^2}}) \simeq \frac{\beta}{c^3}(\frac{v_1^{\,2}}{2} - \frac{v_2^{\,2}}{2}) \qquad . \qquad (20)$$

$$\frac{2\pi}{\lambda_{beat}} = \frac{\beta}{c^3}(v_1 - v_2); \quad V = \frac{\lambda_{beat}}{T_{beat}} = \frac{1}{2}(v_1 + v_2)$$

Their speeds are calculated as

$$v_1 \approx 6100\ (m/s) \quad (\approx \text{observed in Evershed flow})$$
$$v_2 = \omega r_{middle} = 2017\ (m/s) \quad (\text{solar rotation}); \qquad . \qquad (21)$$

Where, regarding Evershed flow as the eruption of the top-layer flow, about 6km/s speed was reported [31]. Alternatively, the top-layer speed v_1 also can be calculated in terms of thermodynamics, to be v_1=6244 (m/s) [28]. Here using v_1=6100 (m/s), their beat period T_{beat} is

calculated to be a very remarkable value of 10.93 (years), in agreement with the sunspot cycle value (say, mean 11 years).

$$T_{beat} \simeq \frac{4\pi c^3}{\beta\left(v_1^{\,2} - v_2^{\,2}\right)} = 10.93\,(years) \quad . \tag{22}$$

The relative error to the mean 11 years is 0.6% for the beat period calculation using the acceleration-roll waves. This beat phenomenon turns out to be a nucleon density oscillation that undergoes to drive the sunspot cycle evolution. The beat wavelength λ_{beat} is too long to observe, only the beat period is easy to be observed. As shown in Fig.9, on the solar surface, the equatorial circumference $2\pi r$ only occupies a little part of the beat wavelength, what we see is the expansion and contraction of the nucleon density.

$$\frac{2\pi r}{\lambda_{beat}} = 0.0031 \quad . \tag{23}$$

This nucleon density oscillation is understood as a new type of nuclear reaction on an astronomic scale.

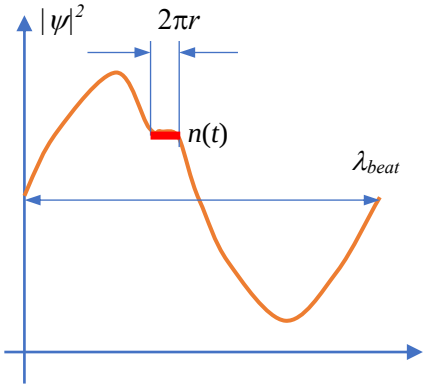

Fig.9 The equatorial circumference 2πr only occupies a little part of the beat wavelength, what we see is the expansion and contraction of the nucleon density.

In the above calculation, although this seems to be a rough model, there is an obvious correlation between solar radius, solar rotation, solar density, ultimate acceleration, and Planck-constant-like constant h.

7. Atmospheric circulation

Consider an acceleration-roll wave ψ_A in the earth shell at the latitude angle A, it will interfere with its neighbor waves within its coherent width. Because the earth shell mainly consists of dense matter, their mutual cascade-interference will cause the acceleration roll wave to have the same phase at the same longitude, so that the acceleration roll wave ψ_A should equal to the $\psi_{equator}$ at the same longitude, as shown in Fig.10(a). This conclusion is supported by the spherical symmetry of the earth's density distribution, that is.

$$\begin{aligned} &\text{spherical symmetry: } \rho(r, A, \varphi) = \rho(r) \quad \Rightarrow \quad \psi(r, A, \varphi) = \psi(r) \\ &\text{or: } \psi_A = \psi_{equator} \end{aligned} \quad . \tag{24}$$

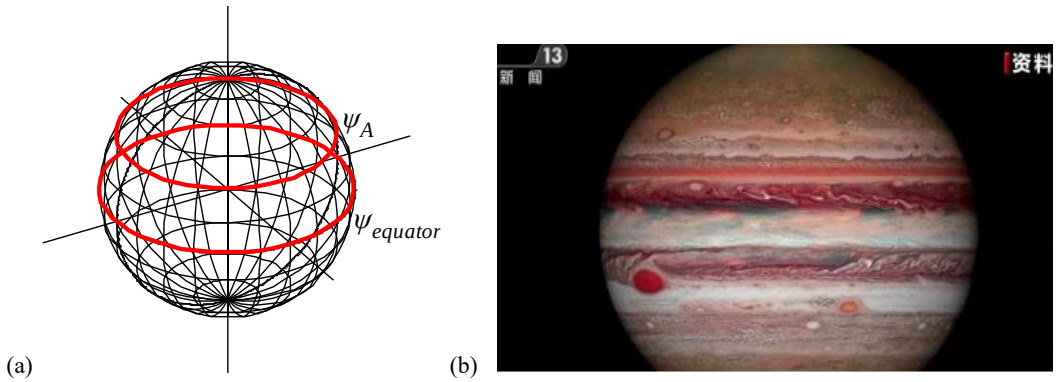

(a) (b)

Fig.10 (a) Mutual cascade-interference will lead to the symmetry of the earth's density distribution. (b) Jupiter (the photo from News).

```
<Clet2020 Script>// [26]
double dP[20],D[2000], r, v1,v2,K1,K2; int i,j,k,N;
int main(){SetViewAngle("temp0,theta60,phi-60");
DrawFrame(FRAME_LINE,1,0xafffaf);Overlook("2,1,60", D);
for(i=0;i<180;i+=15) {k=0; K1=0; K2=i;Grid();}
for(i=0;i<180;i+=15) {k=1; K1=i; K2=0;Grid();}
SetPen(3,0xff0000); k=1; K1=60; K2=0;Grid();K1=90; K2=0; Grid();
//SetPen(3,0x4f4fff); k=1; K1=55; K2=0;Grid();K1=65; K2=0; Grid();
TextHang(40,40,50,"#ifψ#sdA#t"); TextHang(50,40,0,"#ifψ#sdequator#t");
}
Grid(){N=50; K1*=PI/180; K2*=PI/180;    r=60;
if(k==0) {v1=2*PI/N; v2=0;} else {v1=0; v2=2*PI/N;}
for(j=0;j<=N;j+=1){ k=j+j+j;
D[k]=r*sin(K1)*cos(K2);D[k+1]=r*sin(K1)*sin(K2); D[k+2]=r*cos(K1);
K1+=v1;K2+=v2; }Plot("POLYGON,0,50, XYZ,10",D);
}#v07=?>A#t
```

On the contrary, in the thin atmosphere, the cascade-interference within coherence width can be ignored, so the wind and clouds are widely distributed in the sky on a large scale.

Through the coherent width concept, considering the interference between the air ψ_A at the latitude angle A and the shell ψ_{shell} at the same latitude, they are

$$\psi(r,A)=\psi_{air}(r,A)+C\psi_{shell}(r,A)=\psi_{air}(r,A)+C\psi_{shell\_equator}(r)$$

$$T_{beat}\simeq\frac{4\pi c^3}{\beta\left(v_{shell\_equator}{}^2-v_{air}{}^2\right)} \quad . \tag{25}$$

$$v_{shell\_equator}=\omega r$$

$$v_{air}=\omega r\cos(A)+v_{wind}+v_{sun\_effect}$$

where C represents the coupling constant which relates to their distance and mass fractions, their interference leads to a beat phenomenon. Positive wind represents the direction from west to east. The air is subjected to the solar radiation which enforces the beat oscillation to run at the period T_{beat}=1 (year) at the latitude angles A=-23.5°N ~ 23.5°N due to the tilt of the earth axis with respect to the earth's orbital plane. We have known that there is a beat T_{beat}=1year in the first constructive interference ridge with zero wind at the latitude A_1, using the above neat period formula we obtain the sun effect:

$$v_{sun\_effect}=369.788-\omega r\cos(A_1);\quad (units:m/s) \quad . \tag{26}$$

Near the ridge, the sun effect is modified as

$$v_{sun\_effect}=369.788\cos(A-A_1)-\omega r\cos(A) \quad . \tag{27}$$

It is not easy to maintain the constructive interference condition for these waves. When the first

ridge is at latitude A_1=12°N, the wind required for maintaining the beat T_{beat}=1 (year) near the latitude A=12°N is calculated as shown in Fig.11(a) (blue line), this wind will be destroyed by destructive interference at higher latitudes. But, the wind will arise up again at the next locations where the waves satisfy the constructive interference condition: at A=39°N location where beat T_{beat}=0.5 (years), and at A=57°N location where beat T_{beat}=0.37 (years) which is the shortest period that the earth can get within the arctic regions. The maximal wind appears most probably at the midpoint of the first two ridges, about 48m/s. Linking all characteristic points in Fig.11(a) we obtain the predicted wind-curve over the northern hemisphere; this prediction agrees well with the experimental observations at an altitude of 10km (200hPa), as shown in Fig.12.

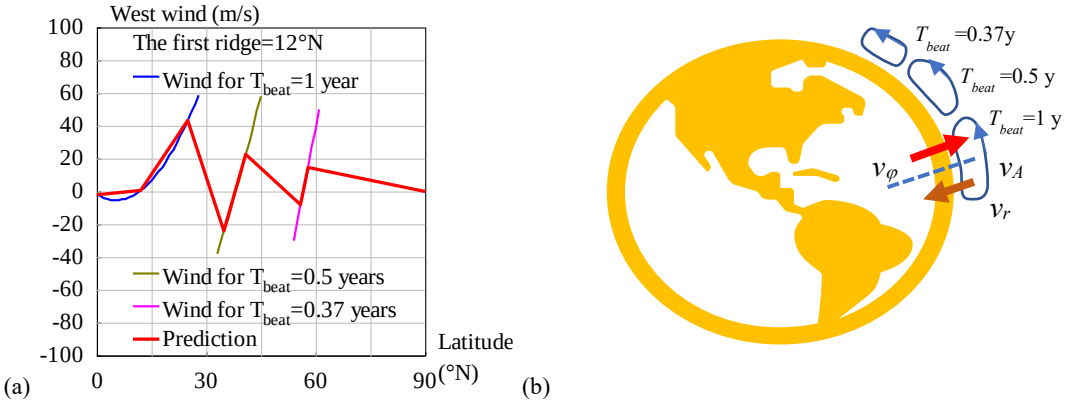

Fig.11 (a) Calculation of west winds in the northern hemisphere. (b) The atmospheric circulation in the northern hemisphere.

```
<Clet2020 Script>// [26]
double beta,H,M,r,rc, rs, rot,v1,v2, Year,T,Lamda,V,a,b,w,Fmax,N[500],S[500],F[100]; int i, j, k, t, m, n, s, f,Type,x;
int main(){beta=1.377075e+14; H=SPEEDC*SPEEDC*SPEEDC/beta;
M=5.97237e24; rs=6.371e6; rot=2*PI/(24*3600); Year=24*3600*365.2422;
Type=1; x=10; if(Type>1) x=-30;//v2=rs*rot; a=v2*v2-4*PI*H/Year; V=sqrt(a)-v2;
if(Type==1)  SetAxis(X_AXIS,0,0,90,"Latitude#n(°N);0;30;60;90;");
else  SetAxis(X_AXIS,-90,-90,90,"Latitude#n(°N);=90;-60;-30;0;30;60;90;");
SetAxis(Y_AXIS,-100,-100,100,"West wind (m/s);-100;-80;-60;-40;-20;0;20;40;60;80;100;");
DrawFrame(0x016a,Type,0xafffaf);//Polyline(2,"-90,0,90,0");
Check(15,k); if(k>24) k=24; if(k<-24) k=-24; //TextAt(100,10,"V=%f",V);
T=Year/2; Wind(); f=0; Findf(); t=N[m+m]; T=Year; Wind(); f=0; Findf();
SetPen(2,0xff); Polyline(n,N,x,70,"Wind for T#sdbeat#t=1 year"); if(Type>1) Polyline(s,S);
F[0]=N[0];F[1]=N[1]; F[2]=N[m+m]; F[3]=N[m+m+1];  t=(t+F[2])/2;//midst of two ridges
 t=t-F[2]+m; Fmax=N[t+t+1]; //TextAt(100,20,"t=%d, Fmax=%f ",t,Fmax);
f=Fmax; Findf(); F[4]=N[m+m]; F[5]=N[m+m+1];
T=Year/2; Wind(); f=-Fmax/2; Findf(); t=m;f=Fmax/2; Findf();
SetPen(2,0x80ff00); Polyline(n,N,x,-50,"Wind for T#sdbeat#t=0.5 years"); if(Type>1) Polyline(s,S);
F[6]=N[t+t]; F[7]=N[t+t+1];  F[8]=N[m+m]; F[9]=N[m+m+1];
T=0.37*Year; Wind(); f=-Fmax/4; Findf(); t=m;f=Fmax/4; Findf();
SetPen(2,0x9933fa); Polyline(n,N,x,-70,"Wind for T#sdbeat#t=0.37 years"); if(Type>1) Polyline(s,S);
F[10]=N[t+t]; F[11]=N[t+t+1];  F[12]=N[m+m]; F[13]=N[m+m+1];  F[14]=90; F[15]=0;
//Draw("ELLIPSE,0,2,XYX,10","15,20,25,35");TextHang(5,40,0,"a route");
SetPen(3,0xff0000); Polyline(8,F,x,-90,"Prediction"); TextHang(x,90,0,"The first ridge=%d°N", k);
}
Wind(){n=0;s=0;
for(i=0;i<90;i+=1)  { a=i*PI/180; b=(i-k)*PI/180; v1=rot*rs*cos(a); v2=rot*rs;
w=369.788*cos(b)-v2*cos(k*PI/180); a=v2*v2-4*PI*H/T; V=sqrt(a)-v1-w;
if(V>-40 && V<60) {N[n+n]=i; N[n+n+1]=V; n+=1;}}
for(i=0;i<90;i+=1)  { a=-i*PI/180; b=(-i-k)*PI/180; v1=rot*rs*cos(a); v2=rot*rs;
w=369.788*cos(b)-v2*cos(k*PI/180); a=v2*v2-4*PI*H/T; V=sqrt(a)-v1-w;
if(V>-40 && V<60) {S[s+s]=-i; S[s+s+1]=V; s+=1;}} }
Findf(){a=1e10; for(i=0;i<n;i+=1)  { b=N[i+i+1]-f ;if(b<0) b=-b;if(b<a) {m=i;a=b;}}
}//if(k==12) ClipJob(APPEND,"i=%d,V=%f",i,V);
#v07=?>A
```

For further improvement of precision, the value of the wind required by the constructive interference condition should be understood as a magnitude, it should be resolved into three components in the spherical coordinates (r,A,φ) as

$$v_{wind}^{\ 2} = v_r^{\ 2} + v_A^{\ 2} + v_\varphi^{\ 2} \ . \tag{28}$$

According to the energy equipartition theorem in thermodynamics, approximately we have the average estimation

$$< v_r^{\,2} >=< v_A^{\,2} >=< v_\varphi^{\,2} >= \frac{1}{3} v_{wind}^{\,2} \ . \tag{29}$$

Thus, the wind vectors around the northern hemisphere of the Earth are plotted in Fig.11(b), the atmospheric circulation consists of three cells: Hadley cell, Ferrel cell, and arctic cell.

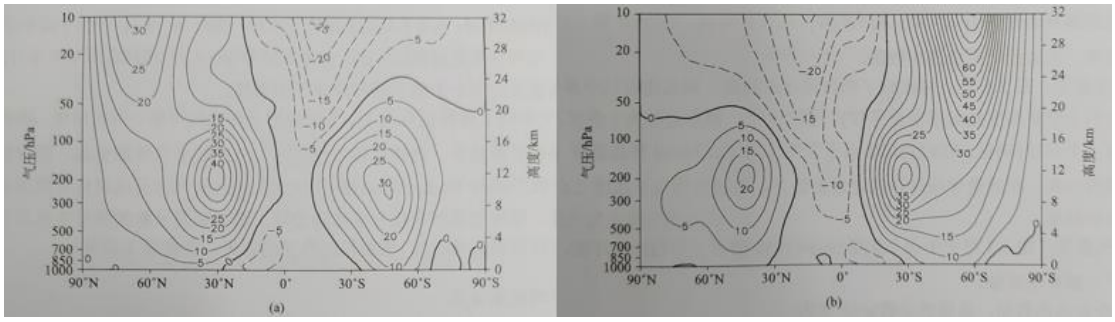

Fig.12 NCEP/NCAR data, mean west winds over 40 years (1958~1997) [36]. (a) in winter; (b) in summer.

The beat T_{beat}=0.5 (years) blows comfortable winds over Europe, Northern America and Northeastern Asia, and modulates the four seasons; the shortest beat T_{beat}=0.37 (years) has a beat wavelength too long to be confined in the arctic regions so that it escapes from the north pole toward the equator, so recognized as the planetary scale waves or Rossby waves.

Since the acceleration-roll wave of the air interferes with the acceleration-roll wave of the earth shell, the easterlies at the equator have a magnitude of about 10 m/s. The trade winds or easterlies are the permanent east-to-west prevailing winds that flow in the Earth's equatorial region. The trade winds blow mainly from the northeast in the Northern Hemisphere and the southeast in the Southern Hemisphere, strengthening during the winter and when the Arctic oscillation is in its warm phase. Trade winds have been used by captains of sailing ships to cross the world's oceans for centuries. The driving force of atmospheric circulation is the uneven distribution of solar heating across the earth, which is greatest near the equator and least at the poles. This air rises to the tropopause, about 10–15 kilometers above sea level, where the air is no longer buoyant [33].

Consider a funny issue, as we have known that v_{sun_effect} =-84(m/s) at the equator when the first ridge at A_1=12°N, imagine if nuclear wars happen on the earth to stop the solar radiation to the earth's surface, then the equatorial wind on the earth's surface will simply reach to -94 (m/s), like the winds on the surfaces of Jupiter and Saturn [28], this will change global climate mode, killed all dinosaurs by strong winds and dusts. Thinking about Mars, Jupiter, and Saturn that gain very weak solar radiation, and there are at least 100 (m/s) strong winds on their surfaces, as shown in Fig.10(b). It tells us how important is the easterly 10 (m/s) at the equator for us, and how important is the air pollution for us. Have you ever gotten an experience: the more serious the air pollution, the stronger the wind? This section helps us understand how the dinosaurs to be buried.

8. Migratory birds

Some birds can migrate regularly to change their habitats with the change of seasons in a year. These birds are called migratory birds. Why do migratory birds migrate? Where do you come from? Where are you going? Will all ethnic groups migrate? Why do some birds migrate farther than others? What mechanism drives migratory birds to migrate at almost a fixed time every year? How do migratory birds migrate in the right direction in the vast sky? And so on, which has always been a subject of great interest to scientists. Behavioral ecology studies the ecological significance of animal behavior; Behavioral ecology often uses cost and benefit to explain why a certain behavior occurs.

The migration route of birds is the area where birds travel between wintering ground and breeding ground. The factors that determine the migration route of birds include terrain, vegetation type, weather, biological characteristics of birds, etc. Traditionally, the migration route must be south-north.

It is found that constructive interference condition takes place at certain latitude where is traditional habitat of migratory birds, so this relativistic approach provides a direction guidance for bird migration. This section clarifies this viewpoint.

(1) A daily closed route to obtain the south-north direction

In spring, the first constructive interference ridge moves to the latitude A=12°N in the northern hemisphere, the wind field is shown in Fig.13.

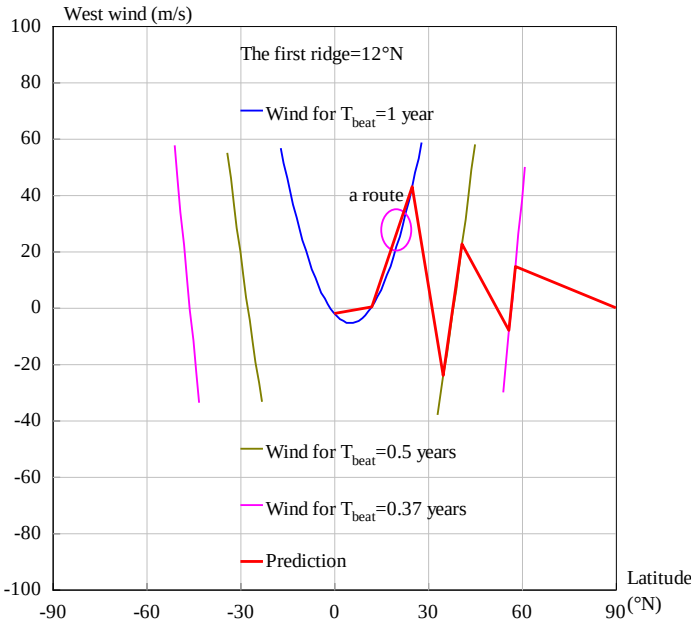

Fig.13 The wind field in spring in the northern hemisphere.

Suppose a bird at its habitat A=20°N makes a flight over a daily closed route, as illustrated in Fig.13 as a closed route near A=20°N, it can easily at once feel the gradient of locate wind field, that indicates the south-north direction. Although the wind field is calculated at a higher altitude (10km), all birds can feel the projection of the wind field at lower altitudes so that they can easily obtain the south-north direction.

(2) Feeling of ridge's latitude change

As shown in Fig.14, from summer to winter, as the latitude of constructive interference ridge

changes, the gradient changes of wind field give all birds a pressure or feeling that undergoes to drive the birds to migrate on time.

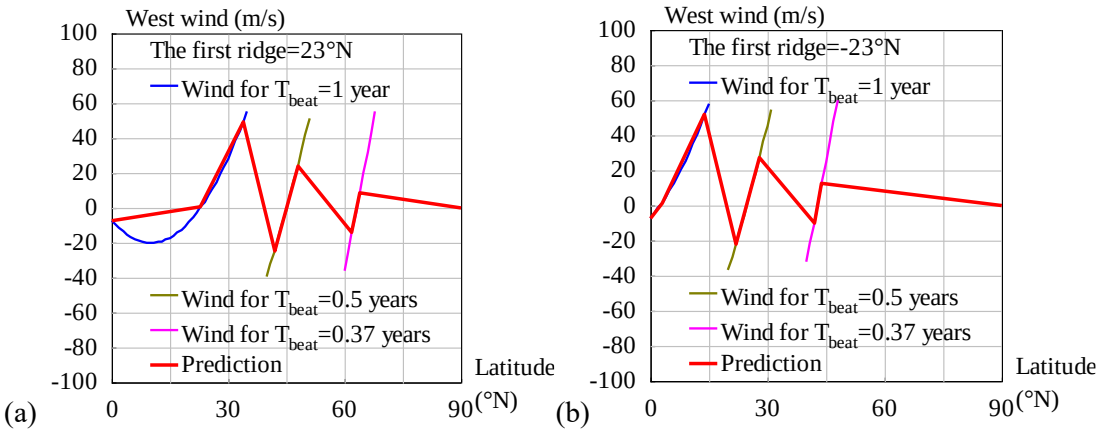

Fig.14 The wind field in (a) summer and (b) winter, the ridges move with the change of seasons.

(3) Two nest zones

To note that there are three easterly zones in the wind field as shown in Fig.13 or 14, where winds are relatively weaker so that the first two zones are suitable for building bird nests, the third is too cold to breed children.

Migratory birds can be divided into summer migratory birds and winter migratory birds. The former refers to flying to a certain area in spring and summer to build a nest and have children. When the young birds grow up, it is late autumn. They successively fly to warmer areas in the south for winter, and then fly to this area for breeding in the spring of the next year. For this area, this kind of birds is called summer migratory birds. Such as the family swallow, it spreads all over China's provinces and cities in summer, and migrates to southern Yunnan, Hainan Island, the Xisha Islands, Taiwan and other places in winter; For example, cuckoo and oriole are also summer migratory birds. The latter refers to wintering in a certain area in winter and flying to the north for breeding in the spring of the next year. When the young birds grow up, they are in late autumn and fly to the original area for wintering. For this area, these birds are called winter migratory birds. For example, wild geese, swans and ducks are winter migratory birds in the middle and lower reaches of the Yangtze River.

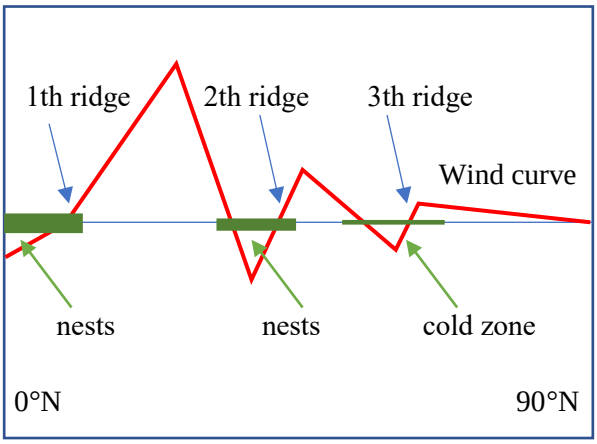

Fig.15 The constructive interference ridges and bird nests.

Actually, as shown in Fig.15, the summer migratory birds favor to construct their nests at lower latitudes, suitable locations are the first easterly zone where the negative west winds are weaker relative to the westerlies. The winter migratory birds favor to construct their nests at higher latitudes, suitable locations are the second easterly zone where the negative west winds are weaker relative to the westerlies. The third easterly zone is so cold that it is not suitable for bird nests.

9. Conclusions

In analogy with the ultimate speed c, there is an ultimate acceleration β, nobody's acceleration can exceed this limit β, in the solar system, β=2.961520e+10(m/s^2). Because this ultimate acceleration is large, any effect related to β will become easy to test, including quantum gravity tests. In this paper, an approach is put forward to connect the ultimate acceleration with quantum theory, and is applied to sunspot problems. The sunspot cycle is calculated to be 10.93 years due to the ultimate acceleration. Due to quantum effect of the ultimate acceleration, the atmospheric constructive interference condition takes place at certain latitudes where are traditional habitats of migratory birds, so this relativistic approach provides a direction guidance for bird migration.

References

[1]C. Marletto, and V. Vedral, Gravitationally Induced Entanglement between Two Massive Particles is Sufficient Evidence of Quantum Effects in Gravity, Phys. Rev. Lett., 119, 240402 (2017)
[2]T. Guerreiro, Quantum effects in gravity waves, Classical and Quantum Gravity, 37 (2020) 155001 (13pp).
[3]S. Carlip, D. Chiou, W. Ni, R. Woodard, Quantum Gravity: A Brief History of Ideas and Some Prospects, International Journal of Modern Physics D, V,24,14,2015,1530028. DOI:10.1142/S0218271815300281.
[4]de Broglie, L., CRAS,175(1922):811-813, translated in 2012 by H. C. Shen in Selected works of de Broglie.
[5]de Broglie, Waves and quanta, Nature, 112, 2815(1923): 540.
[6]de Broglie, Recherches sur la théorie des Quanta, translated in 2004 by A. F. Kracklauer as De Broglie, Louis, On the Theory of Quanta. 1925.
[7]NASA, https://solarscience.msfc.nasa.gov/interior.shtml.
[8]NASA, https://nssdc.gsfc.nasa.gov/planetary/factsheet/marsfact.html.
[9]B. Ryden Introduction to Cosmology, Cambridge University Press, 2019, 2nd edition.
[10]D. Valencia, D. D. Sasselov,R. J. O'Connell, Radius and structure models of the first super-earth planet, The Astrophysical Journal, 656:545-551, 2007, February 10.
[11]D. Valencia, D. D. Sasselov,R. J. O'Connell, Detailed models of super-earths: how well can we infer bulk properties? The Astrophysical Journal, 665:1413–1420, 2007 August 20.
[12]T. Guillot, A. P. Showman, Evolution of "51Pegasusb-like" planets, Astronomy & Astrophysics,2002, 385,156-165, DOI: 10.1051/0004-6361:20011624
[13]T. Guillot, A. P. Showman, Atmospheric circulation and tides of "51Pegasusb-like" planets, Astronomy & Astrophysics,2002, 385,166-180, DOI: 10.1051/0004-6361:20020101
[14]L.N. Fletcher,Y.Kaspi,T. Guillot, A.P. Showman, How Well Do We Understand the Belt/Zone Circulation of Giant Planet Atmospheres? Space Sci Rev, 2020,216:30. https://doi.org/10.1007/s11214-019-0631-9
[15]Y. Kaspi, E. Galanti, A.P. Showman, D. J. Stevenson, T. Guillot, L. Iess, S.J. Bolton, Comparison of the Deep Atmospheric Dynamics of Jupiter and Saturn in Light of the Juno and Cassini Gravity Measurements,Space Sci Rev, 2020, 216:84. https://doi.org/10.1007/s11214-020-00705-7
[16]Orbital Debris Program Office, HISTORY OF ON-ORBIT SATELLITE FRAGMENTATIONS, National Aeronautics and Space Administration, 2018, 15 th Edition.
[17]M. Mulrooney, The NASA Liquid Mirror Telescope, Orbital Debris Quarterly News, 2007, April,v11i2,
[18]Orbital Debris Program Office, Chinese Anti-satellite Test Creates Most Severe Orbital Debris Cloud in History, Orbital Debris Quarterly News, 2007, April,v11i2,
[19]A. MANIS, M. MATNEY, A.VAVRIN, D. GATES, J. SEAGO, P. ANZ-MEADOR, Comparison of the NASA ORDEM 3.1 and ESA MASTER-8 Models, Orbital Debris Quarterly News, 2021, Sept,v25i3.
[20]D. Wright, Space debris, Physics today,2007,10,35-40.
[21]TANG Zhi-mei, DING Zong-hua, DAI Lian-dong, WU Jian, XU Zheng-wen, "The Statistics Analysis of Space

Debris in Beam Parking Model in 78° North Latitude Regions," Space Debris Research, 2017, 17,3, 1-7.
[22]TANG Zhimei DlNG, Zonghua, YANG Song, DAI Liandong, XU Zhengwen, WU Jian The statistics analysis 0f space debris in beam parking model based On the Arctic 500 MHz incoherent scattering radar, CHINESE JOURNAL 0F RADIO SCIENCE, 2018, 25,5, 537-542
[23]TANG Zhimei，DING, Zonghua，DAI Liandong，WU Jian，XU Zhengwen, Comparative analysis of space debris gaze detection based on the two incoherent scattering radars located at 69N and 78N, Chin ．J ．Space Sci, 2018 38,1, 73-78. DOI:10.11728/cjss2018.01.073
[24]DING Zong-hua, YANG Song, JIANG hai, DAI Lian-dong, TANG Zhi-mei, XU Zheng-wen, WU Jian, The Data Analysis of the Space Debris Observation by the Qujing Incoherent Scatter Radar, Space Debris Research, 2018, 18,1, 12-19.
[25]YANG Song, DING Zonghua, Xu Zhengwe, WU Jian, Statistical analysis on the space posture, distribution, and scattering characteristic of debris by incoherent scattering radar in Qujing, Chinese Journal of Radio science, 2018 33,6 648-654, DOI:10.13443/j.cjors.2017112301
[26]Clet Lab, Clet: a C compiler, https://drive.google.com/file/d/1OjKqANcgZ-9V5 6rgcoMtOu9w4rP49sgN/view?usp=sharing
[27]Huaiyang Cui, Relativistic Matter Wave and Its Explanation to Superconductivity: Based on the Equality Principle, Modern Physics, 10,3(2020)35-52. https://doi.org/10.12677/MP.2020.103005
[28]Huaiyang Cui, Relativistic Matter Wave and Quantum Computer, Amazon Kindle eBook, 2021.
[29]Huaiyang Cui, Ultimate Acceleration to Calculate Atomic Spin, viXra:2209.0041, 2022.
[30]Huaiyang Cui, Study of Earthquakes in Japanese Islands Using Quantum Gravity Theory with Ultimate Acceleration, viXra:2209.0149, 2022.
[31]N.Cox, Allen's Astrophysical Quantities, Springer-Verlag, 2001, 4th ed..
[32] S. E. Schneider, T. T. Arny, Pathways to Astronomy, McGraw-Hill Education, 2018, 5th ed.
[33] https://en.wikipedia.org/wiki/El_Ni%C3%B1o%E2%80%93Southern_Oscillation
[34] https://en.wikipedia.org/wiki/Atmosphere_of_Earth
[35] Y.M.Zhu, et al, Principle of Meteorology, China meteorology Press, 2019. p.243.
[36] Liping Li et al, Introduction to Atmospheric Circulation, 2nd edition, Science Press, 2021,
[37] https://en.wikipedia.org/wiki/Tropical_cyclone
[38] https://en.wikipedia.org/wiki/Tropical_cyclone_basins
[39] https://en.wikipedia.org/wiki/pulsar.
[40] L A. Lyne and F. Graham-Smith, Pulsar Astronomy, Fourth Edition, Cambridge University Press, 2012.
[41] Ian Morison, Introduction to Astronomy and Cosmology, John Wiley & Sons, 2008.